ACS APPLIED NANO MATERIALS
Cite This: ACS Appl. Nano Mater. 2018, 1, 2869−2876
Article
www.acsanm.org

Nonthermal Plasma Synthesis of Titanium Nitride Nanocrystals with Plasmon Resonances at Near-Infrared Wavelengths Relevant to Photothermal Therapy

Katelyn S. Schramke,[†,‡] Yunxiang Qin,[†,*,‡] Jacob T. Held,[§] K. Andre Mkhoyan,[§] and Uwe R. Kortshagen*[,‡]

[‡]Department of Mechanical Engineering and [§]Department of Chemical Engineering and Materials Science, University of Minnesota, Minneapolis, Minnesota 55455, United States

Supporting Information

ABSTRACT: Titanium nitride has attracted attention for its plasmonic properties as a thermally stable, biocompatible, and cost-effective alternative to gold. In this work, we synthesized titanium nitride nanocrystals in a nonthermal plasma using tetrakis (dimethylamino) titanium (TDMAT) and ammonia as the titanium and nitrogen precursors. Extinction measurements of as-produced 6−8 nm titanium nitride nanocrystals exhibit a broad plasmon resonance peaking near 800 nm, possibly suitable for photothermal therapy treatments. Ammonia flow rate and plasma power were found to affect nanocrystal morphology and chemical composition, and therefore significantly impact the plasmonic properties. A moderate ammonia flow rate of 1.2 sccm and relatively high nominal plasma power of 100 W produced samples with the best plasmon resonances, narrower than those previously reported for plasma-synthesized titanium nitride nanocrystals.

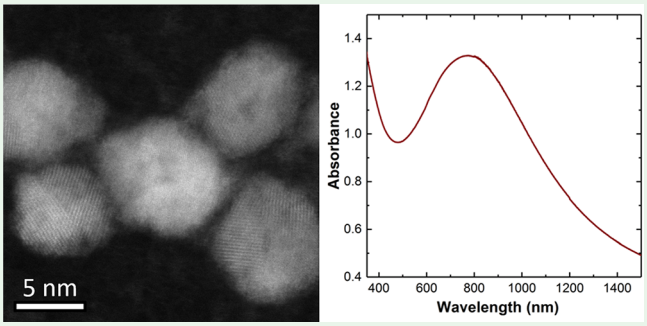

KEYWORDS: *nonthermal plasma, titanium nitride, nanocrystals, near-infrared, plasmonic, photothermal therapy*

Titanium nitride (TiN) has recently attracted interest because of its plasmonic properties.[1−7] Among the potential applications are photothermal therapy treatments (PTTs), for which plasmonic materials must absorb within the biological transparency window from 650 to 1350 nm.[8−10] Most PTT research revolves around gold for its biocompatibility, resistance to oxidation, and ease of solution-phase synthesis. However, the localized surface plasmon resonances (LSPRs) of gold nanospheres depend relatively little on size and peak around 525 nm.[11−14] Hence, more complex geometries such as gold nanorods and nanoshells are used whose main LSPRs can be shifted into the biological transparency window in the near-infrared.[9,15−17] Unfortunately, complex gold nanostructures deform at relatively low temperatures and a minor change in the shape of the gold nanostructures, for example in nanorod aspect ratio, can lead to significant changes in plasmonic properties which can then render the material ineffective.[18,19] In this regard, TiN is more attractive with its high thermal stability and LSPRs in the biological transparency window, even in the form of nanospheres.[5]

Colloidal synthesis techniques, such as those used for gold nanostructures, are typically limited by the boiling points of solvents to relatively low synthesis temperatures.[8,19−21] As such, colloidal techniques may not be suitable for strongly covalently bonded materials such as metal nitrides that require high temperatures to be produced in crystalline form. Gas-phase techniques, on the other hand, are inherently solvent-free and enable significantly higher synthesis temperatures. Indeed, among gas phase methods, nonthermal plasma synthesis of nanomaterials was shown to be capable of producing highly monodisperse nanocrystals (NCs) of covalently bonded materials.[22,23]

Nonthermal plasma synthesis of plasmonic TiN NCs was recently demonstrated by Alvarez Barragan et al.[5] The synthesis relied on titanium tetrachloride and ammonia as titanium and nitrogen precursors, respectively. Although the TiN particles exhibited plasmonic resonances, the precursors used led to the unwanted formation of an ammonium salt that needed to be removed by postsynthesis heating in a furnace. In this paper, we describe the nonthermal plasma synthesis of TiN NCs from ammonia and a different titanium precursor, namely tetrakis (dimethylamino) titanium (TDMAT). As-produced TiN NCs show plasmonic response without postsynthesis treatment, with the best samples produced at moderate ammonia flow rates and relatively high nominal plasma powers exhibiting LSPRs sharper than those previously reported for plasma-synthesized TiN NCs. No noticeable differences in absorption properties

Received: March 27, 2018
Accepted: May 25, 2018
Published: June 7, 2018

DOI: 10.1021/acsanm.8b00505
ACS Appl. Nano Mater. 2018, 1, 2869−2876

are observed for these TiN NCs upon air exposure for up to several days.

EXPERIMENTAL METHODS

The TiN NCs were synthesized in a nonthermal plasma using the same general setup that has been previously described for the production of doped silicon NCs.[24] A schematic of the reactor is shown in Figure 1. In this work, the metal−organic precursor

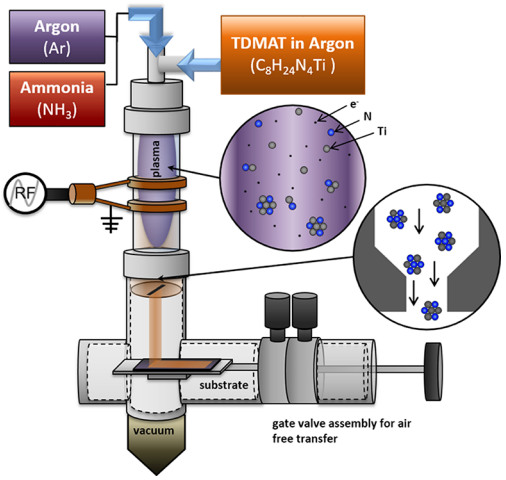

Figure 1. Schematic diagram of the nonthermal plasma setup for the synthesis of TiN NCs.

TDMAT, commonly used in atomic layer deposition or chemical vapor deposition,[25−30] was used as the titanium precursor. The TDMAT is contained in a stainless-steel bubbler and argon is flowed through the TDMAT to carry it to the plasma reactor. TDMAT flow rate was kept constant in the entire study by setting the carrier argon flow at 18 sccm. Because of the low vapor pressure of the metal−organic liquid, the TDMAT process lines and bubbler were heated to 80 and 70 °C, respectively, to prevent condensation inside the reactor or lines. Although TDMAT contains nitrogen atoms, ammonia was used as the nitrogen precursor to allow additional control over nitrogen content. Gas pressure in the plasma region was maintained at 1.6 Torr. TiN NCs are collected in the plasma effluent via impaction onto glass substrates or silicon wafers.

X-ray photoelectron spectroscopy (XPS, Surface Science Laboratories SSX-100) and Fourier-transform infrared spectroscopy (FTIR, Bruker Alpha) measurements were performed to determine chemical composition and surface coverage of the TiN NCs. X-ray diffraction (XRD, Bruker D8 Discover with Co X-ray source) and selective area diffraction (SAD) in transmission electron microscopy (TEM, FEI Tecnai T12) were used to examine the crystallinity of the TiN NCs. TEM (FEI Tecnai T12) and HAADF-STEM (aberration-corrected FEI Titan G2 60−300 STEM operated at 200 kV) images of the TiN NCs deposited directly onto holey carbon TEM grids were collected to study their morphology and size distribution. The UV−vis (Cary 5000 UV−vis spectrophotometer) extinction spectra were taken to study the plasmonic properties of the TiN NCs. Samples are exposed to air during transfer for all the measurements above except for FTIR.

RESULTS AND DISCUSSION

The deposition rate of TiN NCs using the flow-through nonthermal plasma setup was close to 1 mg/min in this study. Produced TiN NCs were consistently around 6−8 nm in diameter under most synthesis conditions used in the present study, i.e., ammonia flow rates between 1.0 and 3.0 sccm, pressure around 1.6 Torr and plasma power between 40 and 100 W. Figure 2a shows a HAADF-STEM image for the TiN NCs produced at 70 W plasma power with a 1.2 sccm ammonia

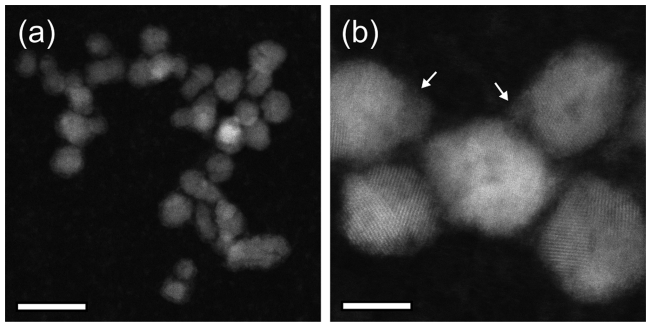

Figure 2. (a) HAADF-STEM image showing the distribution of NC shape and size. (b) Representative HAADF-STEM image of a cluster of NCs showing well-defined lattice fringes of the ∼2−4 nm grains in each NC. Arrows highlight the thin layer of amorphous material on the surface. Scale bars are (a) 20 nm and (b) 5 nm.

flow rate. Higher-resolution HAADF-STEM images (Figure 2b) show that the 6−8 nm NCs consist of numerous 2−4 nm crystallites, covered with a thin (∼1 nm) layer of amorphous material. To avoid confusion, the 2−4 nm crystallites at the core of a NC are hereafter referred to as grains while the entire nanostructure of grains surrounded by a thin amorphous layer is referred to as a NC or simply a particle. Since STEM-EDX mapping of the amorphous layer was experimentally prohibitive due to beam damage and spectrum overlap, FTIR and XPS measurements were performed to evaluate the composition and surfaces of the NCs, as discussed below. The polycrystalline structure suggests that the growth mechanism within the plasma for the TiN NCs is different from those of previously studied plasma-synthesized semiconductor particles where single crystalline particles are usually produced.[31,32] XRD measurements for TiN NCs produced at different plasma powers between 40 and 85 W, shown in Figure 3, reveal that

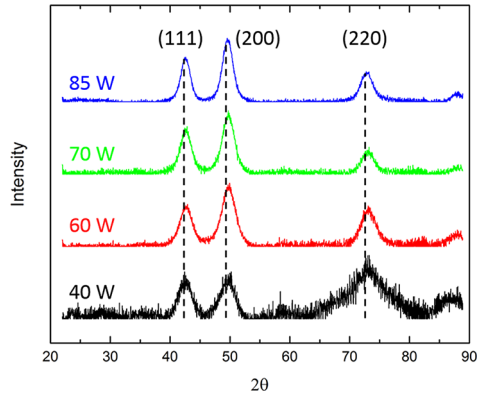

Figure 3. XRD spectra of TiN samples produced at 40, 60, 70, and 85 W plasma power.

TiN grain size only increases slightly from 40 to 60 W nominal plasma power but does not change much above 60 W. Therefore, the TiN NCs are still polycrystalline under high plasma powers. XRD peak positions of all the samples match the TiN reference closely although some minor peak shifts exist. One possible reason for these peak shifts is the presence of size-induced strains in the 2−4 nm TiN grains for which a considerable fraction of atoms reside on the grain surfaces.[33−36] Another possible reason for the peak shifts is the deviation in chemical composition from the perfect stoichiometry, i.e., $TiN_{x=1}$. Studies have shown that the incorporation of nitrogen

DOI: 10.1021/acsanm.8b00505
ACS Appl. Nano Mater. 2018, 1, 2869−2876

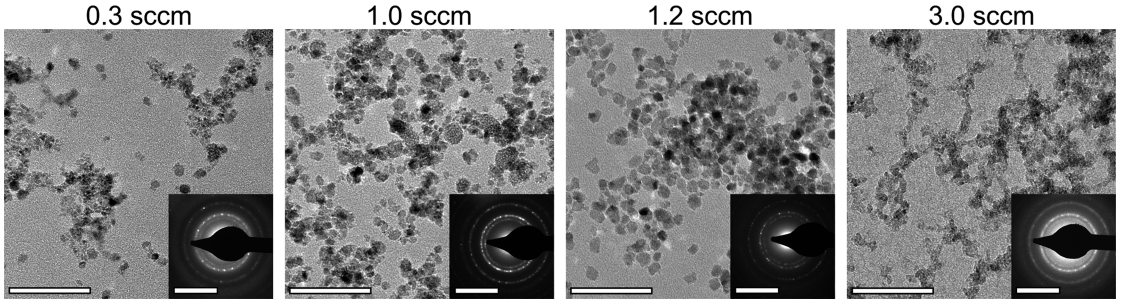

Figure 4. TEM images of TiN samples synthesized at different ammonia flow rates. Insets are SAD patterns of the particles demonstrating crystallinity. Image scale bars are 50 nm; inset scale bars are 4 nm^{-1}.

atoms into the titanium lattice increases lattice spacing in substoichiometric samples, i.e., $TiN_{x<1}$, until the perfect stoichiometry is reached.[37−40] Further nitrogen incorporation in stoichiometric or overstoichiometric samples, i.e., $TiN_{x>1}$, may either increase[37,38] or decrease[39,40] lattice spacing. Since no simple monotonic trends exist for the dependence of lattice spacing on nitrogen atomic percentage, no conclusions can be drawn from the XRD spectra on whether the TiN grains are substoichiometric or overstoichiometric even if stoichiometry is the sole contributor to peak shifts. Finally, it should be noted that similar XRD peak shifts have been observed before in polycrystalline TiN thin films.[41,42]

Among the different plasma parameters, ammonia flow rate and plasma power are found to greatly affect the particle morphology, chemical composition, and optical properties of the TiN NCs. TEM images were collected for TiN samples produced at 100 W nominal plasma power with different ammonia flow rates, shown in Figure 4. At very low ammonia flow rates, e.g., around 0.3 sccm, the particle morphology varies significantly and there are few larger particles and many smaller nonuniform nanocrystalline structures. As ammonia flow rate is increased to around 1.0 sccm, the nonuniform structures begin to disappear, leaving behind TiN NCs with a tighter size distribution. The most monodispersed TiN NCs are found at 1.2 sccm. Then, as ammonia flow rate is further increased, the monodispersity starts to deteriorate again and eventually the particles lose their defined shape at around 3.0 sccm.

The elemental composition of the TiN NCs was measured using XPS. Ammonia flow rate is set at 1.2 sccm based on the TEM results, whereas the synthesis plasma power is varied between 70 and 100 W. Survey XPS scans confirm the presence of titanium, nitrogen, carbon, and oxygen in all samples (shown in Figure S1). The TiN NCs are nitrogen rich, exhibiting Ti:N atomic ratios close to 1:2 at low plasma powers (<70 W) and 3:4 at high plasma powers (>75 W). They also consistently contain a high atomic percentage of carbon (~40%). Assuming a near-stoichiometric TiN crystalline core (consisting of many grains), supported by the XRD spectra (Figure 3), this indicates surplus nitrogen and carbon atoms near the surface of the particles, possibly forming several disordered atomic layers. FTIR measurements were made in a nitrogen purged glovebox to examine this hypothesis and to study what bonds are present at the TiN NC surface. As can be seen in Figure 5, the FTIR spectrum of the NCs confirms the existence of several carbon and nitrogen bonds at the sample surface. The hydrogen bonds shown in the FTIR come from the methyl groups in TDMAT. TiN samples produced with different plasma parameters all have FTIR spectra similar to Figure 5.

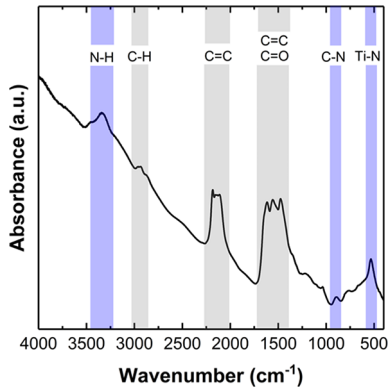

Figure 5. Typical FTIR of TiN NCs exhibiting peaks from N−H,[43,44] C−H,[45] C═C,[44,46] C═O,[47] C−N,[45] and Ti−N[46] bonds at the surface of the NCs.

Although it is safe to assume that most carbon originates from the methyl groups in the titanium precursor and some from handling the samples in air, it is still unclear how TDMAT breaks down within the capacitively coupled plasma used in the present study and, specifically, whether, and how much nitrogen within the TDMAT molecule contributes to the TiN NC growth. It should be noted that previous studies on TiN synthesis via remote electron cyclotron resonance plasma elegantly demonstrated that the vast majority of the nitrogen in their TiN films comes from plasma-activated nitrogen precursor (N_2 or NH_3) rather than TDMAT.[48,49]

A recent study suggested that the commonly used binding energy reference in XPS measurements, the C 1s peak of adventitious carbon, may vary significantly over different transition metal nitride films and that even the same transition metal material, e.g., TiN films, can have random variations up to 0.5 eV between different samples.[50] Therefore, C 1s peak of adventitious carbon at ~285 eV is used only as a rough binding energy reference in this study. High-resolution XPS spectra of carbon, shown in Figure 6, indicate the presence of titanium carbide (TiC, ~282.1 eV[51−54]) for TiN samples produced at plasma powers higher than or equal to 75 W. As electron temperature in the plasma is mostly a function of the reactor geometry and pressure, this suggests that the formation of TiC is favored at high electron densities. For samples containing the TiC phase, the binding energy of TiC is used as a secondary binding energy reference. Indeed, despite the C 1s peaks of adventitious carbon having a binding energy difference of up to 0.5 eV between different samples, the TiC phase remains very close to 282.1 eV and therefore no compensating chemical shifts are applied in XPS spectra fitting.

DOI: 10.1021/acsanm.8b00505
ACS Appl. Nano Mater. 2018, 1, 2869−2876

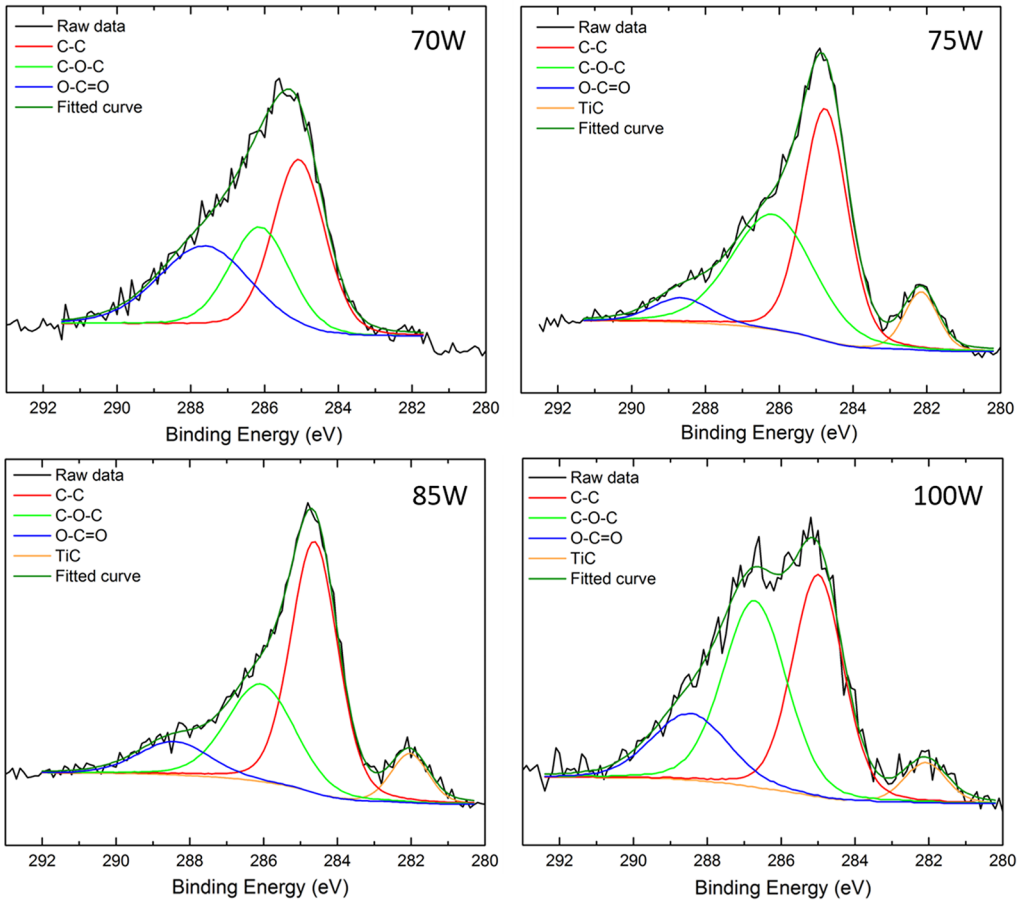

Figure 6. High-resolution C 1s spectra for samples produced with 70, 75, 85, and 100 W plasma power. Ammonia flow rate is 1.2 sccm for all samples.

High-resolution XPS scans of the Ti 2p peaks are then fitted with three sets of doublets at 70 W and four sets of doublets at 75, 85, and 100 W, shown in Figure 7. The doublets at 70 W contain a TiN phase, a titanium dioxide (TiO_2) phase and an intermediate phase of titanium oxynitride (TiON). The doublets at 75, 85, and 100 W contain an extra phase of TiC. During XPS data fitting, the area ratio of Ti 2p doublets (Area $2p_{3/2}$: Area $2p_{1/2}$) are targeted at 2:1 but are not always satisfied exactly. The complexity of Ti 2p spectra arising from multiple phases positioned close to each other and possible shakeup features was well documented[55,56] and may lead to imperfect fittings in some cases. Nevertheless, extensive effort was made in this study to meet the constraints on peak position, doublet separation and doublet area ratio simultaneously as much as possible. It should be noted that centering the TiN $2p_{3/2}$ peak at around 455.85 eV,[51,57−67] near the upper limit of the possible range, produced the best fitting overall for our data, even though some studies have fitted the same peak to around 455.3 eV.[51,68−72] In addition, when the difference in the C−C binding energy between the values in this study (284.6−285.1 eV for samples produced at plasma powers at or above 75 W) and the value suggested in the detailed study on adventitious carbon contamination on TiN films (284.52 eV)[50] is considered, the binding energy of the TiN $2p_{3/2}$ peak is brought closer to 455.3 eV while the binding energies of other phases still fall within the possible ranges. The TiC, TiON, and TiO_2 $2p_{3/2}$ peaks are fitted to center around 455.1,[52−54,73] 457.2,[61,74,75] and 458.5 eV.[76−79]

On the basis of the high-resolution Ti 2p spectra fitting, samples produced at or above 75 W contain significantly less TiO_2, and the highest TiN percentage (phase percentage of TiN among all Ti-containing phases, same below), ∼40%, is achieved at 100 W. However, the 100 W samples still contain ∼15% TiO_2 and ∼30% TiON phases. This suggests that the titanium located at the disordered surface of the NCs may readily oxidize to form TiON and TiO_2. NCs of various materials synthesized via nonthermal plasma have been reported to have a crystalline core and up to a nanometer of amorphous surface,[22] which agrees with our observations in Figure 2.

Extinction spectra of the TiN NCs were measured with the NCs directly deposited onto a borosilicate glass substrate to study their plasmonic properties, shown in Figures 8. Background spectrum of a bare borosilicate substrate has been subtracted from all sample spectra. The TiN NCs were produced with 100 W nominal plasma power and different ammonia flow rates between 0.3 to 3.0 sccm. They exhibit LSPRs in the range of 770 to 800 nm which is within the biological transparency window, making the TiN NCs produced in this study conducive to PTT applications. We should note, however, that the LSPRs from gold nanorods can be of much higher intensity.[80] Figure 8b shows the dependence on ammonia flow. At very low ammonia flow rates (0.3 sccm), no LSPR is present due to the broad size distribution and nonuniformity of the NCs produced with 0.3 sccm of ammonia, confirmed by TEM in Figure 4. As ammonia flow rate is

DOI: 10.1021/acsanm.8b00505
ACS Appl. Nano Mater. 2018, 1, 2869−2876

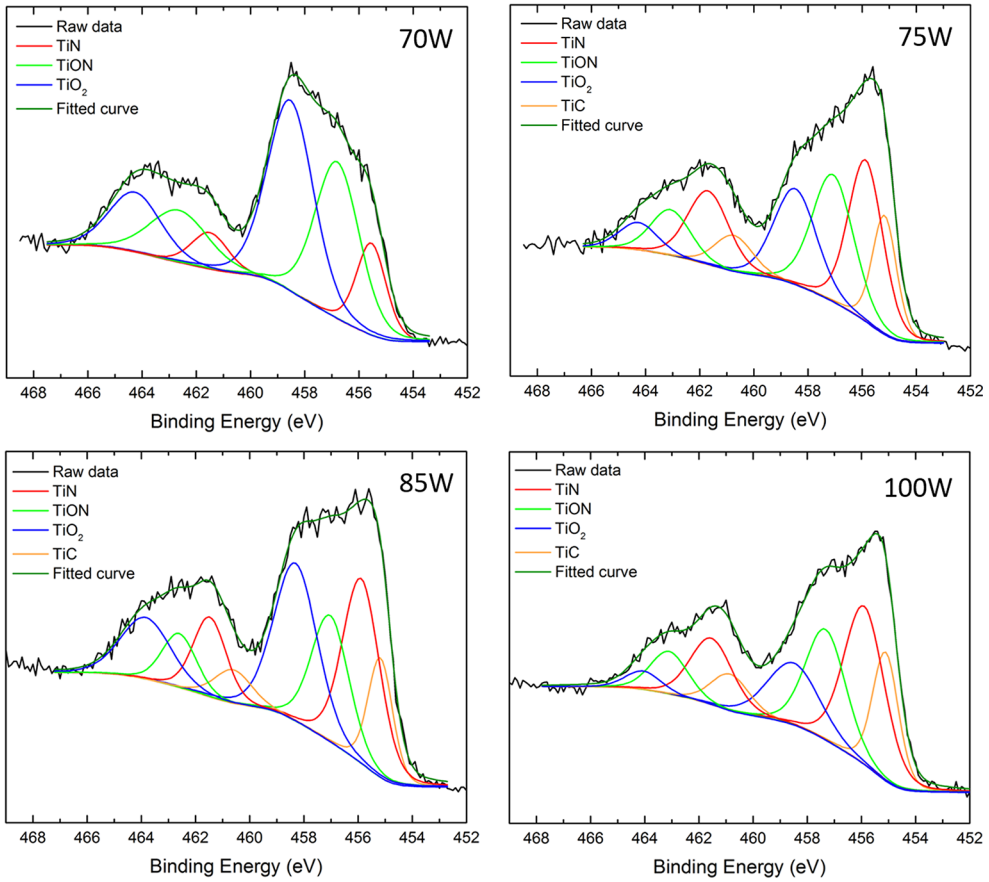

Figure 7. High-resolution Ti 2p spectra for samples produced with 70, 75, 85, and 100 W plasma power. Ammonia flow rate is 1.2 sccm for all samples.

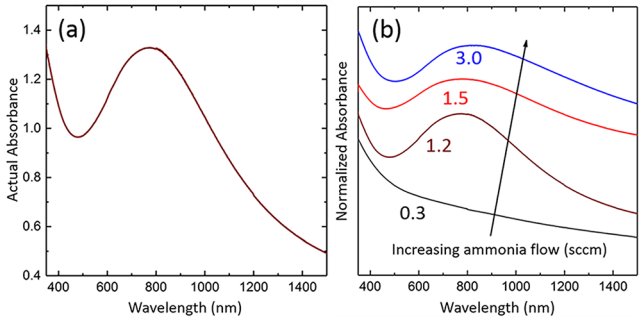

Figure 8. UV−vis spectra showing the LSPR of the TiN NCs; (a) a spectrum showing the actual extinction from samples produced at 1.2 sccm ammonia flow rate and (b) stacked spectra showing the change in LSPR with ammonia flow rates from 0.3 sccm where no plasmon is observed to 3.0 sccm where a broadened plasmon is observed. Arrow shows the slight LSPR redshift with increasing NH_3 flow rate. The sharpest LSPR is observed at a moderate ammonia flow rate of 1.2 sccm. All samples are produced at 100 W plasma power.

increased to 1.2 sccm, resulting in a more monodipersed distribution of TiN NCs, a sharp LSPR narrower than that previously reported for plasma synthesized TiN NCs is observed.[5] The actual spectrum without normalization is shown in Figure 8a. Further increase in the ammonia flow rate to 1.5 and 3.0 sccm causes the LSPR to broaden and slightly redshift as the TiN NCs start to lose their defined shape and uniform size. No noticeable differences in LSPRs are observed for these TiN NCs upon air exposure for several days.

CONCLUSION

Plasmonic TiN NCs were successfully synthesized via non-thermal plasma synthesis using the metal−organic titanium precursor TDMAT and ammonia. The observed LSPR was in a similar location to that of the gold nanorods suitable for PTT, although it should be noted that the LSPRs from gold nanorods can have much higher intensity. NCs size uniformity and optimized elemental composition are shown to be crucial for good plasmonic behavior. Therefore, the width and presence of the LSPR are found to be dependent on the ammonia flow rate and plasma power as are the uniformity and composition of the NCs. A moderate ammonia flow rate of 1.2 sccm and relatively high nominal plasma power of 100 W proved to be the best experimental condition for the LSPR, which has a narrower shape than the previously reported LSPR for plasma-produced TiN.

ASSOCIATED CONTENT

Supporting Information

The Supporting Information is available free of charge on the ACS Publications website at DOI: 10.1021/acsanm.8b00505.

Figure S1, typical XPS survey scan of TiN samples showing the presence of titanium, oxygen, nitrogen and carbon (PDF)

AUTHOR INFORMATION

Corresponding Authors

*E-mail: qinxx157@umn.edu.

DOI: 10.1021/acsanm.8b00505
ACS Appl. Nano Mater. 2018, 1, 2869−2876

*E-mail: kortshagen@umn.edu.

ORCID

Yunxiang Qin: 0000-0003-1636-3976
Jacob T. Held: 0000-0003-3864-4314
K. Andre Mkhoyan: 0000-0003-3568-5452
Uwe R. Kortshagen: 0000-0001-5944-3656

Author Contributions

†K.S.S. and Y.Q. contributed equally to this work

Notes

The authors declare no competing financial interest.

■ ACKNOWLEDGMENTS

The work of K.S.S., Y.Q., and U.R.K. was supported by the Army Office of Research under MURI Grant W911NF-12-1-0407. The work of J.T.H. and K.A.M. was supported by MRSEC program of the National Science Foundation under Award DMR-1420013. Part of this work was carried out in the College of Science and Engineering Characterization Facility, University of Minnesota, which has received capital equipment funding from the NSF through the UMN MRSEC program under Award DMR-1420013. Part of this work also used the College of Science and Engineering Minnesota Nanocenter, University of Minnesota, which receives partial support from NSF through the NNIN program.

■ REFERENCES

(1) Cortie, M.; Giddings, J.; Dowd, A. Optical Properties and Plasmon Resonances of Titanium Nitride Nanostructures. *Nanotechnology* **2010**, *21*, 115201.
(2) Naik, G. V.; Kim, J.; Boltasseva, A. Oxides and Nitrides as Alternative Plasmonic Materials in the Optical Range. *Opt. Mater. Express* **2011**, *1*, 1090−1099.
(3) Naik, G. V.; Schroeder, J. L.; Ni, X.; Kildishev, A. V.; Sands, T. D.; Boltasseva, A. Titanium Nitride as a Plasmonic Material for Visible and Near-Infrared Wavelengths. *Opt. Mater. Express* **2012**, *2*, 478−489.
(4) Ishii, S.; Shinde, S. L.; Jevasuwan, W.; Fukata, N.; Nagao, T. Hot Electron Excitation from Titanium Nitride Using Visible Light. *ACS Photonics* **2016**, *3*, 1552−1557.
(5) Alvarez Barragan, A.; Ilawe, N. V.; Zhong, L.; Wong, B. M.; Mangolini, L. A Non-Thermal Plasma Route to Plasmonic TiN Nanoparticles. *J. Phys. Chem. C* **2017**, *121*, 2316−2322.
(6) Kaur, M.; Ishii, S.; Shinde, S. L.; Nagao, T. All-ceramic Microfibrous Solar Steam Generator: TiN Plasmonic Nanoparticle-loaded Transparent Microfibers. *ACS Sustainable Chem. Eng.* **2017**, *5*, 8523−8528.
(7) Shinde, S. L.; Ishii, S.; Dao, T. D.; Sugavaneshwar, R. P.; Takei, T.; Nanda, K. K.; Nagao, T. Enhanced Solar Light Absorption and Photoelectrochemical Conversion Using TiN Nanoparticle-Incorporated C_3N_4−C Dot Sheets. *ACS Appl. Mater. Interfaces* **2018**, *10*, 2460−2468.
(8) Dickerson, E. B.; Dreaden, E. C.; Huang, X.; El-Sayed, I. H.; Chu, H.; Pushpanketh, S.; McDonald, J. F.; El-Sayed, M. A. Gold Nanorod Assisted Near-Infrared Plasmonic Photothermal Therapy (PPTT) of Squamous Cell Carcinoma in Mice. *Cancer Lett.* **2008**, *269*, 57−66.
(9) Chen, H.; Shao, L.; Li, Q.; Wang, J. Gold Nanorods and Their Plasmonic Properties. *Chem. Soc. Rev.* **2013**, *42*, 2679−2724.
(10) Huang, X.; Jain, P. K.; El-Sayed, I. H.; El-Sayed, M. A. Plasmonic Photothermal Therapy (PPTT) Using Gold Nanoparticles. *Lasers Med. Sci.* **2008**, *23*, 217.
(11) Eustis, S.; El-Sayed, M. A. Why Gold Nanoparticles Are More Precious Than Pretty Gold: Noble Metal Surface Plasmon Resonance and Its Enhancement of the Radiative and Nonradiative Properties of Nanocrystals of Different Shapes. *Chem. Soc. Rev.* **2006**, *35*, 209−217.
(12) Qiao, L.; Wang, D.; Zuo, L.; Ye, Y.; Qian, J.; Chen, H.; He, S. Localized Surface Plasmon Resonance Enhanced Organic Solar Cell with Gold Nanospheres. *Appl. Energy* **2011**, *88*, 848−852.
(13) Huang, X.; Qian, W.; El-Sayed, I. H.; El-Sayed, M. A. The Potential Use of the Enhanced Nonlinear Properties of Gold Nanospheres in Photothermal Cancer Therapy. *Lasers Surg. Med.* **2007**, *39*, 747−753.
(14) Orendorff, C. J.; Sau, T. K.; Murphy, C. J. Shape-Dependent Plasmon-Resonant Gold Nanoparticles. *Small* **2006**, *2*, 636−639.
(15) Li, J.; Guo, H.; Li, Z.-Y. Microscopic and Macroscopic Manipulation of Gold Nanorod and Its Hybrid Nanostructures. *Photonics Res.* **2013**, *1*, 28−41.
(16) Melancon, M. P.; Lu, W.; Yang, Z.; Zhang, R.; Cheng, Z.; Elliot, A. M.; Stafford, J.; Olson, T.; Zhang, J. Z.; Li, C. In Vitro and in Vivo Targeting of Hollow Gold Nanoshells Directed at Epidermal Growth Factor Receptor for Photothermal Ablation Therapy. *Mol. Cancer Ther.* **2008**, *7*, 1730−1739.
(17) Kim, J.; Park, S.; Lee, J. E.; Jin, S. M.; Lee, J. H.; Lee, I. S.; Yang, I.; Kim, J.-S.; Kim, S. K.; Cho, M.-H.; Hyeon, T. Designed Fabrication of Multifunctional Magnetic Gold Nanoshells and Their Application to Magnetic Resonance Imaging and Photothermal Therapy. *Angew. Chem.* **2006**, *118*, 7918−7922.
(18) Yang, J.; Kramer, N. J.; Schramke, K. S.; Wheeler, L. M.; Besteiro, L. V.; Hogan, C. J., Jr; Govorov, A. O.; Kortshagen, U. R. Broadband Absorbing Exciton−Plasmon Metafluids with Narrow Transparency Windows. *Nano Lett.* **2016**, *16*, 1472−1477.
(19) Nikoobakht, B.; El-Sayed, M. A. Preparation and Growth Mechanism of Gold Nanorods (NRs) Using Seed-Mediated Growth Method. *Chem. Mater.* **2003**, *15*, 1957−1962.
(20) Xu, L.; Kuang, H.; Wang, L.; Xu, C. Gold Nanorod Ensembles as Artificial Molecules for Applications in Sensors. *J. Mater. Chem.* **2011**, *21*, 16759−16782.
(21) Khatua, S.; Paulo, P. M.; Yuan, H.; Gupta, A.; Zijlstra, P.; Orrit, M. Resonant Plasmonic Enhancement of Single-Molecule Fluorescence by Individual Gold Nanorods. *ACS Nano* **2014**, *8*, 4440−4449.
(22) Mangolini, L.; Thimsen, E.; Kortshagen, U. High-Yield Plasma Synthesis of Luminescent Silicon Nanocrystals. *Nano Lett.* **2005**, *5*, 655−659.
(23) Kortshagen, U. R.; Sankaran, R. M.; Pereira, R. N.; Girshick, S. L.; Wu, J. J.; Aydil, E. S. Nonthermal Plasma Synthesis of Nanocrystals: Fundamental Principles, Materials, and Applications. *Chem. Rev.* **2016**, *116*, 11061−11127.
(24) Kramer, N. J.; Schramke, K. S.; Kortshagen, U. R. Plasmonic Properties of Silicon Nanocrystals Doped with Boron and Phosphorus. *Nano Lett.* **2015**, *15*, 5597−5603.
(25) Lee, Y. J. Low-Impurity, Highly Conformal Atomic Layer Deposition of Titanium Nitride Using NH_3-Ar-H_2 Plasma Treatment for Capacitor Electrodes. *Mater. Lett.* **2005**, *59*, 615−617.
(26) Yun, J.-Y.; Park, M.-Y.; Rhee, S.-W. Comparison of Tetrakis (dimethylamido) Titanium and Tetrakis (diethylamido) Titanium as Precursors for Metallorganic Chemical Vapor Deposition of Titanium Nitride. *J. Electrochem. Soc.* **1999**, *146*, 1804−1808.
(27) Musschoot, J.; Xie, Q.; Deduytsche, D.; Van den Berghe, S.; Van Meirhaeghe, R.; Detavernier, C. Atomic Layer Deposition of Titanium Nitride from TDMAT Precursor. *Microelectron. Eng.* **2009**, *86*, 72−77.
(28) Yun, J.-H.; Choi, E.-S.; Jang, C.-M.; Lee, C.-S. Effect of Post-Treatments on Atomic Layer Deposition of TiN Thin Films Using Tetrakis (dimethylamido) Titanium and Ammonia. *Jpn. J. Appl. Phys.* **2002**, *41*, L418.
(29) Kim, J. Y.; Choi, G. H.; Do Kim, Y.; Kim, Y.; Jeon, H. Comparison of TiN Films Deposited Using Tetrakisdimethylaminotitanium and Tetrakisdiethylaminotitanium by the Atomic Layer Deposition Method. *Jpn. J. Appl. Phys.* **2003**, *42*, 4245.
(30) Elam, J.; Schuisky, M.; Ferguson, J.; George, S. Surface Chemistry and Film Growth During TiN Atomic Layer Deposition Using TDMAT and NH_3. *Thin Solid Films* **2003**, *436*, 145−156.
(31) Gresback, R.; Holman, Z.; Kortshagen, U. Nonthermal Plasma Synthesis of Size-Controlled, Monodisperse, Freestanding Germanium Nanocrystals. *Appl. Phys. Lett.* **2007**, *91*, 093119.

DOI: 10.1021/acsanm.8b00505
ACS Appl. Nano Mater. 2018, 1, 2869−2876

(32) Bapat, A.; Anderson, C.; Perrey, C. R.; Carter, C. B.; Campbell, S. A.; Kortshagen, U. Plasma Synthesis of Single-Crystal Silicon Nanoparticles for Novel Electronic Device Applications. Plasma Phys. *Plasma Phys. Controlled Fusion* **2004**, *46*, B97.
(33) Palosz, B.; Grzanka, E.; Gierlotka, S.; Stelmakh, S.; Pielaszek, R.; Bismayer, U.; Neuefeind, J.; Weber, H.-P.; Proffen, Th.; Von Dreele, R.; Palosz, W. Analysis of Short and Long Range Atomic Order in Nanocrystalline Diamonds with Application of Powder Diffractometry. *Z. Kristallogr. - Cryst. Mater.* **2002**, *217*, 497−509.
(34) Gilbert, B.; Huang, F.; Zhang, H.; Waychunas, G. A.; Banfield, J. F. Nanoparticles: Strained and Stiff. *Science* **2004**, *305*, 651−654.
(35) Ouyang, G.; Li, X.; Tan, X.; Yang, G. Size-induced Strain and Stiffness of Nanocrystals. *Appl. Phys. Lett.* **2006**, *89*, 031904.
(36) Brat, T.; Parikh, N.; Tsai, N.; Sinha, A.; Poole, J.; Wickersham, C., Jr Characterization of Titanium Nitride Films Sputter Deposited from a High-Purity Titanium Nitride Target. *J. Vac. Sci. Technol., B: Microelectron. Process. Phenom.* **1987**, *5*, 1741−1747.
(37) Kang, J. H.; Kim, K. J. Structural, Optical, and Electronic Properties of Cubic TiN_x Compounds. *J. Appl. Phys.* **1999**, *86*, 346−350.
(38) Duan, G.; Zhao, G.; Wu, L.; Lin, X.; Han, G. Structure, Electrical and Optical Properties of TiN_x Films by Atmospheric Pressure Chemical Vapor Deposition. *Appl. Surf. Sci.* **2011**, *257*, 2428−2431.
(39) Lee, Y.-K.; Kim, J.-Y.; Lee, Y.-K.; Lee, M.-S.; Kim, D.-K.; Jin, D.-Y.; Nam, T.-H.; Ahn, H.-J.; Park, D.-K. Surface Chemistry of Non-stoichiometric TiN_x Films Grown on (1 0 0) Si Substrate by DC Reactive Magnetron Sputtering. *J. Cryst. Growth* **2002**, *234*, 498−504.
(40) Sundgren, J.-E.; Johansson, B.-O.; Karlsson, S.-E.; Hentzell, H. Mechanisms of Reactive Sputtering of Titanium Nitride and Titanium Carbide II: Morphology and Structure. *Thin Solid Films* **1983**, *105*, 367−384.
(41) Merie, V.; Pustan, M.; Negrea, G.; Bîrleanu, C. Research on Titanium Nitride Thin Films Deposited by Reactive Magnetron Sputtering for MEMS Applications. *Appl. Surf. Sci.* **2015**, *358*, 525−532.
(42) Dobrzański, L. A.; Golombek, K. Structure and Properties of Selected Cemented Carbides and Cermets Covered with TiN/(Ti, Al, Si)N/TiN Coatings Obtained by the Cathodic Arc Evaporation Process. *Mater. Res.* **2005**, *8*, 113−116.
(43) Miller, P. J.; Colson, S. D.; Chupka, W. A. Observation of the $\nu_1 + n\nu_2$ Combination Band in the $\tilde{C}'^1A_1$ Rydberg State of NH_3. *Chem. Phys. Lett.* **1988**, *145*, 183−187.
(44) Afanasyev-Charkin, I.; Nastasi, M. Hard Si−N−C Coatings Produced by Pulsed Glow Discharge Deposition. *Surf. Coat. Technol.* **2004**, *186*, 108−111.
(45) Dubois, L. H.; Zegarski, B. R.; Girolami, G. S. Infrared Studies of the Surface and Gas Phase Reactions Leading to the Growth of Titanium Nitride Thin Films from Tetrakis (dimethylamido) Titanium and Ammonia. *J. Electrochem. Soc.* **1992**, *139*, 3603−3609.
(46) Huang, S.; Tour, J. M. Rapid Solid-Phase Synthesis of Oligo (1, 4-Phenylene Ethynylene) S by a Divergent/convergent Tripling Strategy. *J. Am. Chem. Soc.* **1999**, *121*, 4908−4909.
(47) Oliveira, C.; Gonçalves, L.; Almeida, B.; Tavares, C.; Carvalho, S.; Vaz, F.; Escobar Galindo, R.; Henriques, M.; Susano, M.; Oliveira, R. XRD and FTIR Analysis of Ti-Si-C-ON Coatings for Biomedical Applications. *Surf. Coat. Technol.* **2008**, *203*, 490−494.
(48) Weber, A.; Nikulski, R.; Klages, C.-P.; Gross, M.; Charatan, R.; Opilan, R.; Brown, W. Aspects of TiN and Ti Deposition in an ECR Plasma Enhanced CVD Process. *Appl. Surf. Sci.* **1995**, *91*, 314−320.
(49) Weber, A.; Klages, C.-P.; Gross, M.; Charatan, R.; Brown, W. Formation Mechanism of TiN by Reaction of Tetrakis (dimethylamido)-Titanium with Plasma-Activated Nitrogen. *J. Electrochem. Soc.* **1995**, *142*, L79−L82.
(50) Greczynski, G.; Hultman, L. C 1s Peak of Adventitious Carbon Aligns to the Vacuum Level: Dire Consequences for Material's Bonding Assignment by Photoelectron Spectroscopy. *ChemPhysChem* **2017**, *18*, 1507.
(51) Chastain, J.; King, R. C.; Moulder, J. *Handbook of X-Ray Photoelectron Spectroscopy: A Reference Book of Standard Spectra for Identification and Interpretation of XPS Data*; Physical Electronics Division, Perkin-Elmer Corporation: Eden Prairie, MN, 1992.
(52) Delplancke-Ogletree, M.-P.; Monteiro, O. R. Deposition of Titanium Carbide Films from Mixed Carbon and Titanium Plasma Streams. *J. Vac. Sci. Technol., A* **1997**, *15*, 1943−1950.
(53) Ignaszak, A.; Song, C.; Zhu, W.; Zhang, J.; Bauer, A.; Baker, R.; Neburchilov, V.; Ye, S.; Campbell, S. Titanium Carbide and Its Core-Shelled Derivative TiC@TiO_2 as Catalyst Supports for Proton Exchange Membrane Fuel Cells. *Electrochim. Acta* **2012**, *69*, 397−405.
(54) Kiran, V.; Kalidindi, S. B.; Jagirdar, B. R.; Sampath, S. Electrochemical Oxidation of Boron Containing Compounds on Titanium Carbide and Its Implications to Direct Fuel Cells. *Electrochim. Acta* **2011**, *56*, 10493−10499.
(55) Saha, N. C.; Tompkins, H. G. Titanium Nitride Oxidation Chemistry: An X-Ray Photoelectron Spectroscopy Study. *J. Appl. Phys.* **1992**, *72*, 3072−3079.
(56) Vasile, M.; Emerson, A.; Baiocchi, F. The Characterization of Titanium Nitride by X-Ray Photoelectron Spectroscopy and Rutherford Backscattering. *J. Vac. Sci. Technol., A* **1990**, *8*, 99−105.
(57) Jung, M. J.; Nam, K. H.; Chung, Y. M.; Boo, J. H.; Han, J. G. The Physiochemical Properties of TiO_xN_y Films with Controlled Oxygen Partial Pressure. *Surf. Coat. Technol.* **2003**, *171*, 71−74.
(58) Balogun, M.-S.; Yu, M.; Li, C.; Zhai, T.; Liu, Y.; Lu, X.; Tong, Y. Facile Synthesis of Titanium Nitride Nanowires on Carbon Fabric for Flexible and High-Rate Lithium Ion Batteries. *J. Mater. Chem. A* **2014**, *2*, 10825−10829.
(59) Lim, B. K.; Park, H. S.; See, A. K.; Liu, E. Z.; Wu, S. H. Comparison of in Situ and Ex Situ Plasma-Treated Metalorganic Chemical Vapor Deposition Titanium Nitride Thin Films. *J. Vac. Sci. Technol., B: Microelectron. Process. Phenom.* **2002**, *20*, 2219−2224.
(60) Greczynski, G.; Mráz, S.; Schneider, J.; Hultman, L. Substantial Difference in Target Surface Chemistry Between Reactive Dc and High Power Impulse Magnetron Sputtering. *J. Phys. D: Appl. Phys.* **2018**, *51*, 05LT01.
(61) Yu, M.; Zhao, S.; Feng, H.; Hu, L.; Zhang, X.; Zeng, Y.; Tong, Y.; Lu, X. Engineering Thin MoS_2 Nanosheets on TiN Nanorods: Advanced Electrochemical Capacitor Electrode and Hydrogen Evolution Electrocatalyst. *ACS Energy Lett.* **2017**, *2*, 1862−1868.
(62) Gonzalez-Valenzuela, C.; Cota, L.; Gonzalez-Valenzuela, R.; de la Cruz, W.; Duarte-Möller, A. Study by AES of the Titanium Nitruration in the Growing of TiN Thin Films by PLD Technique. *Appl. Surf. Sci.* **2006**, *252*, 3401−3405.
(63) Popoola, O.; Denanot, M.; Moine, P.; Villain, J.; Cahoreau, M.; Caisso, J. Microstructural and Analytical Characterization of TiN_x Precipitation in N+ Implanted Equiatomic NiTi Alloys. *Acta Metall.* **1989**, *37*, 867−876.
(64) Hayashida, T.; Endo, K.; Liu, Y.; Kamei, T.; Matsukawa, T.; Sakamoto, K.; Tsukada, J.; Ishikawa, Y.; Yamauchi, H.; Ogura, A.; et al. Investigation of Thermal Stability of TiN Film Formed by Atomic Layer Deposition Using Tetrakis (dimethylamino) Titanium Precursor for Metal-Gate Metal−Oxide−Semiconductor Field-Effect Transistor. *Jpn. J. Appl. Phys.* **2010**, *49*, 04DA16.
(65) Braic, M.; Balaceanu, M.; Vladescu, A.; Kiss, A.; Braic, V.; Epurescu, G.; Dinescu, G.; Moldovan, A.; Birjega, R.; Dinescu, M. Preparation and Characterization of Titanium Oxy-Nitride Thin Films. *Appl. Surf. Sci.* **2007**, *253*, 8210−8214.
(66) Chu, S.-Z.; Inoue, S.; Wada, K.; Hishita, S.; Kurashima, K. Self-Organized Nanoporous Anodic Titania Films and Ordered Titania Nanodots/nanorods on Glass. *Adv. Funct. Mater.* **2005**, *15*, 1343−1349.
(67) Roca-Ayats, M.; García, G.; Galante, J.; Peña, M.; Martínez-Huerta, M. Electrocatalytic Stability of Ti Based-Supported Pt_3 Ir Nanoparticles for Unitized Regenerative Fuel Cells. *Int. J. Hydrogen Energy* **2014**, *39*, 5477−5484.
(68) Wang, Y.; Yuan, H.; Lu, X.; Zhou, Z.; Xiao, D. All Solid-State PH Electrode Based on Titanium Nitride Sensitive Film. *Electroanalysis* **2006**, *18*, 1493−1498.

DOI: 10.1021/acsanm.8b00505
ACS Appl. Nano Mater. 2018, 1, 2869−2876

(69) Shen, Y.; Liu, Z.; Jiang, N.; Zhang, H.; Chan, K.; Xu, Z. Effect of Silicon Addition on Surface Morphology and Structural Properties of Titanium Nitride Films Grown by Reactive Unbalanced Direct Current-Magnetron Sputtering. *J. Mater. Res.* **2004**, *19*, 523−534.
(70) Corneille, J.; Chen, P.; Truong, C.; Oh, W.; Goodman, D. Surface Spectroscopic Studies of the Deposition of TiN Thin Films from Tetrakis-(dimethylamido)-Titanium and Ammonia. *J. Vac. Sci. Technol., A* **1995**, *13*, 1116−1120.
(71) Lu, F.-H.; Chen, H.-Y. XPS Analyses of TiN Films on Cu Substrates After Annealing in the Controlled Atmosphere. *Thin Solid Films* **1999**, *355*, 374−379.
(72) Tang, D.; Yi, R.; Gordin, M. L.; Melnyk, M.; Dai, F.; Chen, S.; Song, J.; Wang, D. Titanium Nitride Coating to Enhance the Performance of Silicon Nanoparticles as a Lithium-Ion Battery Anode. *J. Mater. Chem. A* **2014**, *2*, 10375−10378.
(73) Girolami, G. S.; Jensen, J. A.; Pollina, D. M.; Allocca, C. M.; Kaloyeros, A. E.; Williams, W. S. Organometallic Route to the Chemical Vapor Deposition of Titanium Carbide Films at Exceptionally Low Temperatures. *J. Am. Chem. Soc.* **1987**, *109*, 1579−1580.
(74) Avasarala, B.; Haldar, P. Electrochemical Oxidation Behavior of Titanium Nitride Based Electrocatalysts Under PEM Fuel Cell Conditions. *Electrochim. Acta* **2010**, *55*, 9024−9034.
(75) Yang, T.-S.; Yang, M.-C.; Shiu, C.-B.; Chang, W.-K.; Wong, M.-S. Effect of N_2 Ion Flux on the Photocatalysis of Nitrogen-Doped Titanium Oxide Films by Electron-Beam Evaporation. *Appl. Surf. Sci.* **2006**, *252*, 3729−3736.
(76) Li, L.; Yan, J.; Wang, T.; Zhao, Z.-J.; Zhang, J.; Gong, J.; Guan, N. Sub-10 Nm Rutile Titanium Dioxide Nanoparticles for Efficient Visible-Light-Driven Photocatalytic Hydrogen Production. *Nat. Commun.* **2015**, *6*, 5881.
(77) Scanlon, D. O.; Dunnill, C. W.; Buckeridge, J.; Shevlin, S. A.; Logsdail, A. J.; Woodley, S. M.; Catlow, C. R. A.; Powell, M. J.; Palgrave, R. G.; Parkin, I. P.; et al. Band Alignment of Rutile and Anatase TiO_2. *Nat. Mater.* **2013**, *12*, 798−801.
(78) O'Neill, S. A.; Clark, R. J.; Parkin, I. P.; Elliott, N.; Mills, A. Anatase Thin Films on Glass from the Chemical Vapor Deposition of Titanium (IV) Chloride and Ethyl Acetate. *Chem. Mater.* **2003**, *15*, 46−50.
(79) Anpo, M.; Nakaya, H.; Kodama, S.; Kubokawa, Y.; Domen, K.; Onishi, T. Photocatalysis over Binary Metal Oxides. Enhancement of the Photocatalytic Activity of Titanium Dioxide in Titanium-Silicon Oxides. *J. Phys. Chem.* **1986**, *90*, 1633−1636.
(80) Huang, X.; El-Sayed, I. H.; Qian, W.; El-Sayed, M. A. Cancer Cell Imaging and Photothermal Therapy in the Near-infrared Region by Using Gold Nanorods. *J. Am. Chem. Soc.* **2006**, *128*, 2115−2120.

DOI: 10.1021/acsanm.8b00505
ACS Appl. Nano Mater. 2018, 1, 2869−2876